CHEMISTRY OF MATERIALS
Article

Chem. Mater. **2010,** *22,* 4821–4827 4821
DOI:10.1021/cm1011235

Nanoscale SnO_2 Hollow Spheres and Their Application as a Gas-Sensing Material

Fabian Gyger,[†] Michael Hübner,[‡] Claus Feldmann,*[,†] Nicolae Barsan,[‡] and Udo Weimar*[,‡]

[†]*Institut für Anorganische Chemie, Karlsruhe Institute of Technology, Engesserstrasse 15, D-76131 Karlsruhe, Germany, and* [‡]*Institut für Physikalische und Theoretische Chemie, Universität Tübingen, Auf der Morgenstelle 15, D-72076 Tübingen, Germany*

Received August 4, 2009. Revised Manuscript Received July 2, 2010

The use of nanoscale SnO_2 hollow spheres as a redox-active sensor is investigated. The underlying hollow spheres are prepared via a microemulsion approach and exhibit an outer diameter of about 15−25 nm, a highly crystalline shell with a thickness of 3−5 nm and an inner cavity of 10−20 nm in diameter. Subsequent to materials characterization based on SEM, STEM, TEM, IR, TG, BET, and XRD the applicability of as-prepared hollow spheres as highly porous layers in sensor operation is tested. Accordingly, SnO_2 hollow spheres deposited on common sensor substrates show a good response to CO in a concentration range of 50 to 300 ppm. Moreover, the material turned out to be useful as a model system to study the conduction model of a porous layer with small grains.

Introduction

SnO_2 is generally well-known as a wide bandgap *n*-type semiconductor and has been used as an efficient sensor material already.[1] Its conductivity is related to the presence of intrinsic oxygen vacancies. According to previous studies, gas sensors based on SnO_2 have found application especially in the detection of toxic gases such as CO.[2] State-of-the-art sensors are based on polycrystalline thick films of SnO_2 with noble-metal additives. These base materials are generally synthesized via wet-chemistry processes and exhibit crystallite sizes in the order of 8−100 nm.[3] The resulting thick films are porous and agglomerated, which makes the understanding of sensing quite difficult.[4] The overall sensor conductance is determined by surface reactions and the charge transfer processes between the adsorbed species and the semiconductor (proper sensing). Herein the adsorbate will modulate the concentration of the free charges available for the overall conduction process (transduction). The more complicated the morphology of the layer, the more difficult the interpretation and modeling of the sensing/transduction. To this concern, nanoscale SnO_2 hollow spheres can have a couple of advantages, which are making them very interesting candidates as a model system.

Porous oxide nanostructures in general and hollow spheres in particular are known and used in gas sensing; for an overview, see ref 5. What differentiates the nanostructures we use here is the fact that the shell is not polycrystalline and that the inner cavity is much below 100 nm. In contrast, previous studies concern to agglomeration of nanoparticles organized in porous structures with comparably low specific surface (typically $< 80\,m^2\,g^{-1}$) or to porous structures that were gained by thermal decomposition of solid organic−inorganic hybrid precursors without using any nanoparticles.[6] From this point of view the hollow spheres we're presenting here are qualitatively different. Nanoscale SnO_2 hollow spheres are here prepared based on a microemulsion approach, which gives access to nanoscale hollow spheres of various materials, including metals, oxides and sulfides.[7−9]

Keeping in mind that the shell of the hollow sphere is accessible to gases from both, the outside and the inside, and taking into account that its crystalline quality is very good, one can consider that individual hollow spheres are mimicking very thin single crystals. This fact makes the modeling of conduction in the shells less complicate and may allow for a more simple comparison between experimental results and theory. This is a very intriguing fact and makes the investigations of that type of material interesting. Besides that, their geometry opens up new

*Corresponding author. Phone: ++49-721-6082855 (C.F.); +49-7071-2978766 (U.W.). Fax: ++49-721-6084892 (C.F.); ++49-7071-295960 (U.W.). E-mail: claus.feldmann@kit.edu (C.F.); nb@ipc.uni-tuebingen.de (U.W.).

(1) Göpel, W.; Schierbaum, K. D. *Sens. Actuators, B* **1995**, *26/27*, 1.
(2) Hauptmann, P. *Sensors Principles and Applications*; Prentice Hall: Upper Saddle River, NJ, 1991; pp 115−124.
(3) Weimar, U. Habilitation Thesis, University of Tübingen, Tübingen, Germany, 2001.
(4) Barsan, N.; Weimar, U. *J. Electroceram.* **2001**, *7*, 143.
(5) Lee, J. H. *Sens. Actuators, B* **2009**, *140*, 319.
(6) Hagemeyer, A.; Hogan, Z.; Schlichter, M.; Smaka, B.; Streukens, G.; Turner, H.; Volpe, A.; Weinberg, H.; Yaccato, K. *Appl. Catal., A* **2007**, *317*, 139.
(7) Zimmermann, C.; Feldmann, C.; Wanner, M.; Gerthsen, D. *Small* **2007**, *3*, 1347.
(8) Buchold, D. H. M.; Feldmann, C. *Nano Lett.* **2007**, *7*, 3489.
(9) Gröger, H.; Gyger, F.; Leidinger, P.; Zurmühl, C.; Feldmann, C. *Adv. Mater.* **2009**, *21*, 1586.

Published on Web 07/22/2010

ways for adding noble metal sensitizers in the form of supported or supporting catalysts.

Experimental Section

Synthesis of SnO_2 Hollow Spheres. Samples were prepared in a water-in-oil (w/o)- microemulsion established by dissolving 1.82 g of cetyltrimethylammoniumbromide (CTAB, Aldrich, 95%) as a surfactant and 5.0 mL of hexanol (Fluka, >98%) as a cosurfactant in 50.0 mL of *n*-dodecane (Aldrich, >99%) as the nonpolar oil phase. In addition, 2.0 mL of a 5:1 mixture of methanol (Seulberger, 99%) and demineralized water were added. To this micellar system was added dropwise 10 mL of a 0.01 M solution of $Sn(Ot\text{-}Bu)_4$ (ABCR, 99.99%) in dodecane within 1 h at ambient temperature (20 °C) without stirring. Subsequently, the reaction mixture was left to react for 12 h. Accordingly, hydrolysis of the tin alcoholate occurred at the liquid-to-liquid phase boundary. Thus, hollow spheres encapsulating the polar phase were established. By adding 20 mL of diethylene glycol (DEG) the reaction was terminated. The SnO_2 hollow spheres were separated by centrifugation. Finally, the resulting colorless precipitate was washed three times with ethanol by resuspending and centrifugation. The solid material was then redispersed in ethanol.

Analytical Techniques. Scanning electron microscopy (SEM) was conducted on a Zeiss Supra 40 VP, using an acceleration voltage of 3−30 kV and a working distance of 4 mm. SEM samples were prepared by evaporation of suspensions in DEG on a silicon wafer. Scanning transmission electron microscopy (STEM) was conducted on a Zeiss Supra 40 VP, too, using an acceleration voltage up to 30 kV and a working distance of 4 mm. STEM samples were prepared by 4 h vacuum-evaporation of droplets of SnO_2 hollow spheres in ethanol on a holey carbon-film copper-grid at 120 °C. Transmission electron microscopy (TEM) was performed with a Philips CM200 FEG/ST microscope at an acceleration voltage of 200 kV. Samples were prepared by deposition and evaporation of an ethanolic SnO_2 dispersion on a lacey-film Cu grid. X-ray powder diffraction (XRD) was carried out with a Stoe STADI-P diffractometer operating with Ge-monochromatized Cu−Kα radiation. Brunauer−Emmett−Teller (BET) analysis of as-prepared powder samples was carried out with a BELSORP mini II, applying N_2 as adsorbate. Fourier-transform infrared (FT-IR) spectra were recorded with a Vertex 70 FT-IR spectrometer from Bruker Optics. The transmittance of pellets consisted of 1 mg of the powder sample and 150 mg KBr, and was measured in a wavenumber interval of 370−7000 cm^{-1}. Differential thermal analysis/thermogravimetry (DTA-TG) was performed with a NETZSCH STA 409C applying α-Al_2O_3 as a crucible material as well as a reference sample. The samples were heated under N_2 flow to 600 °C with a heating rate of 5 K min^{-1}.

Sensor Fabrication and Measuring Principle. The sensing layer was produced simply via dip-coating of an emulsion of SnO_2 hollow spheres in ethanol with a capillary on a planar Al_2O_3 substrate. The front side of the alumina substrate was provided with interdigitated electrodes onto which the material was deposited. A Pt heater on the backside allowed the sensor to operate at well-controlled temperatures. For the sensing DC electrical measurements were performed by using an electronic circuitry which ensured a constant voltage drop over the sensing layer. To monitor the response to several CO concentrations, we connected the sensor, mounted in a chamber, to a multimeter (Keithley DMM 199). The gas concentrations and the flow of 200 mL min^{-1} were adjusted by a computer controlled gas mixing system. The carrier gas was synthetic air with 50% relative humidity (room temperature) in the background. The sensing experiments were operated at 300 and 350 °C.

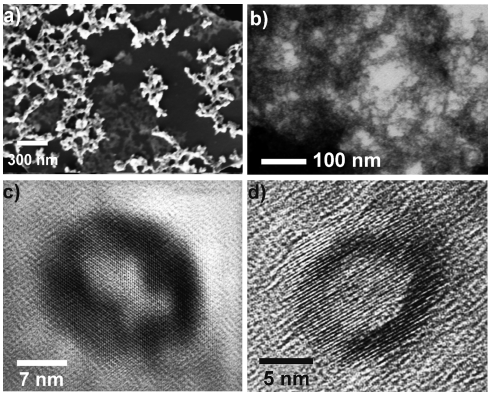

Figure 1. Overview (a) SEM, (b) STEM, and (c, d) HRTEM images of as-prepared SnO_2 hollow spheres indicating diameter, wall thickness, and inner cavity as well as the crystallinity of the sphere wall.

Results and Discussion

Materials Synthesis and Characterization. Subsequent to microemulsion-based synthesis and careful washing procedures, as-prepared SnO_2 hollow spheres were obtained as a colorless fine powder. To elucidate particle size, morphology, and structure, this powder was first investigated by electron microscopy. Overview scanning transmission electron microscopy (STEM) images show a variety of particles with diameters of 15−25 nm (Figure 1a, b), most of which beeing agglomerated as a powder. Some single nonagglomerated particles already indicate the presence of an inner cavity even at this level of magnification. HRTEM (high-resolution transmission electron microscopy) images reveal hollow spheres with a diameter of 15−25 nm (Figure 1c, d). In detail, wall thicknesses of 3−5 nm and an inner diameter of 10−20 nm are visible. Because TEM analysis only allows investigating a limited number of particles, it can not be excluded that at least some filled particles as well as some destructed hollow spheres are present, too. According to HRTEM, the sphere walls are highly crystalline (Figure 1c, d). When considering that the synthesis was performed at ambient temperature, this finding is quite surprising because oxides such as SnO_2 normally tend to crystallize at elevated temperatures (>200 °C).[10] The observed highly ordered lattice fringes with a *d*-value of 3.3 Å (Figure 1c) correspond very well to reference data (SnO_2/cassiterite: (110) with 3.35 Å).[11] Surprisingly, some hollow spheres exhibit a significantly reduced d-value of 2.8 Å (Figure 1d), which only matches the fluorite-type high-pressure modification of SnO_2 (at 21 GPa: (111) with 2.8 Å).[12,13] This is observed for those hollow spheres with smaller diameters (typically below 20 nm). This finding can be ascribed to a certain internal pressure of the highly crystalline, but

(10) West, A. R. *Solid State Chemistry and Its Applications*; Wiley: Chichester, U.K., 1990; pp 318−358.
(11) Bolzan, A. A.; Fong, C.; Kennedy, B. J.; Howard, C. J. *Acta Crystallogr., Sect. B* **1997**, *53*, 373.
(12) Haines, J.; Léger, J. M.; Schulte, O. *Science* **1996**, *271*, 629.
(13) Haines, J.; Léger, J. M. *Phys. Rev. B* **1997**, *55*, 11144.

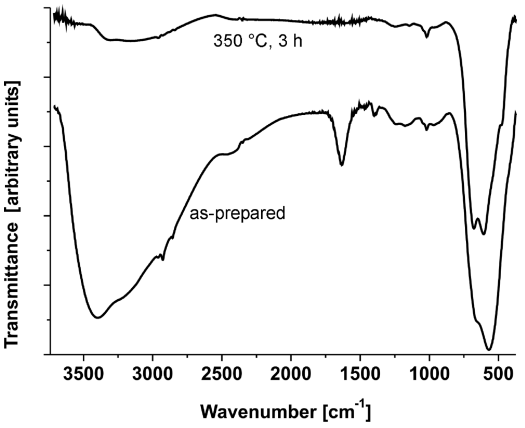

Figure 2. FT-IR spectra of as-prepared SnO_2 hollow spheres and the material after careful drying (350 °C, 3 h).

strongly curved shell and should be the more favored the smaller the spheres are. Indeed, such an effect has been described already for carbon onions. Here the internal pressure was proven to exceed 38 GPa, which results in a phase transition of graphite to diamond at a temperature of 700 °C.[14−16] With regard to as-prepared SnO_2 hollow spheres, it remains unclear until now whether the herein observed phase transition originates from the synthesis itself, or whether it was triggered by electron-beam-induced heating or charging.

Because the shell formation of SnO_2 hollow spheres was conducted at the water-to-oil phase boundary of water-filled micelles, the as-prepared material is expected to contain large quantities of water. Accordingly, infrared spectroscopy was involved (Figure 2a). FT-IR spectra of as-prepared samples indeed show very strong vibrations at 3650−3350 and 1600−1550 cm^{-1}, which can be related to ν(O−H) and δ(O−H), respectively.[17] Vibrations at 2950−2800 cm^{-1} (i.e., ν(C−H)) and at 1400−900 cm^{-1} (i.e., δ(C−H)) can be ascribed to minor amounts of residual surfactant. Moreover, a broad and intense vibration at 750−400 cm^{-1} can be ascribed to the Sn−O lattice vibration of SnO_2.[18,19] To examine the temperature-driven removal of the volatiles, we conducted thermogravimetry (Figure 3). To this end, a continuous weight loss of about 18% in sum was observed to occur up to a temperature of 400 °C. Partly this finding can be explained by surface-bound water, methanol, hexanol, or CTAB stemming from the microemulsion synthesis. However, detailed studies with compact nanoparticles that have been prepared similarly in microemulsion systems only show 1−5% of weight loss due to adhesion of volatiles on the particle surface.[9,20,21] The here observed massive loss in weight can only be ascribed when taking significant quantities of water inside the hollow spheres into account.

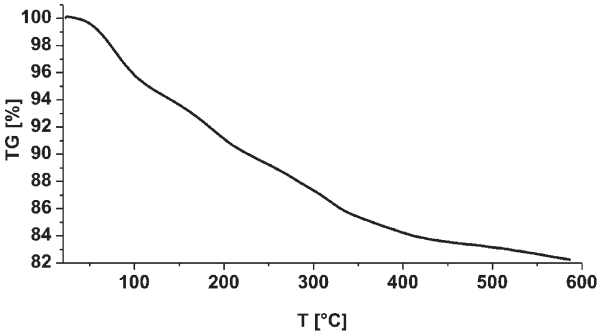

Figure 3. Thermogravimetry of as-prepared SnO_2 hollow spheres (total weight: 38.2 mg).

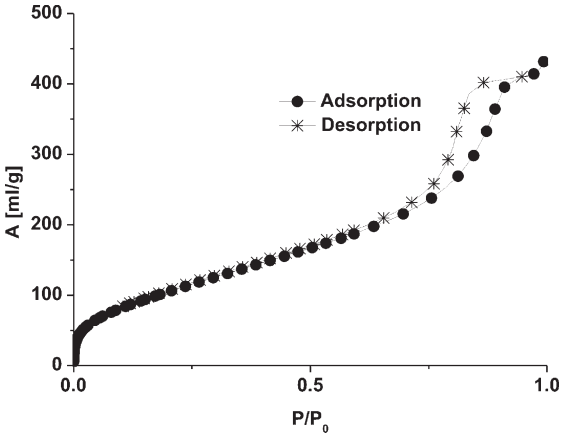

Figure 4. Nitrogen sorption of vacuum-dried nanoscale SnO_2 hollow spheres.

In view of the sensor operation temperature, as-prepared SnO_2 hollow spheres were therefore carefully dried for 3 h at 350 °C in air. As indicated by FT-IR spectra (Figure 2b), the amount of water—deduced from the intensity of ν(O−H)—as well as all other organic molecules (e.g., ethanol, CTAB) are now completely vanished.

A powder that consists of nanoscale hollow spheres suggests a large specific surface area. This is verified by nitrogen adsorption analysis and calculation of the specific surface area by means of the Brunauer−Emmett−Teller (BET) method (Figure 4). Indeed, the carefully dried and evacuated powder exhibits a specific surface of 417 $m^2\ g^{-1}$. Note that this value would require particle diameters below 5 nm if dense particles were assumed.[22] With regard to the observed diameter of 15−25 nm of as-prepared SnO_2 a considerable inner surface is in sufficient agreement with the observed value and confirms the presence of cavities. In addition to the extended surface, a certain hysteresis between adsorption and desorption of nitrogen is observed. With the assumption of a kinetically hindered gas transport through the sphere wall this finding is to expected and hints to an inner cavity, too. Note also that SnO_2 nanoparticles with comparable specific surfaces (i.e., 400−500 $m^2\ g^{-1}$), but compact morphology and diameter of 3−5 nm do show no or a much less pronounced hysteresis.[23] Altogether, both findings − the

(14) Banhart, F.; Ajayan, P. M. *Nature* **1996**, *382*, 433.
(15) Zaiser, M.; Banhart, F. *Phys. Rev. Lett.* **1997**, *79*, 3680.
(16) Huang, J. Y. *Nano Lett.* **2007**, *7*, 2335.
(17) Günzler, H.; Böck, H. *IR-Spektroskopie*; VCH: Weinheim, Germany, 1988.
(18) Gervais, F.; Kress, W. *Phys. Rev. B* **1985**, *31*, 4809.
(19) Katiyar, R. S.; Dawson, P.; Hargreave, M. M.; Wilkinson, G. R. *J. Phys. C* **1971**, *4*, 2421.
(20) Buchold, D. H. M.; Feldmann, C. *Chem. Mater.* **2007**, *19*, 3376.
(21) Buchold, D. H. M.; Feldmann, C. *Adv. Funct. Mater.* **2008**, *18*, 1002.
(22) Lide, D. R. *Handbook of Chemistry and Physics*; CRC Press: Boca Raton, FL, 2008.

extended surface as well as the hysteresis − are well in agreement with the presence of nanoscale hollow spheres and confirms the vast majority of particles to exhibit an inner cavity.

On the basis of its morphology and its extensive surface, the material becomes interesting for sensor application. Because typical sensors operate at temperatures of 250−350 °C, the thermal behavior of the SnO_2 hollow spheres was investigated based by X-ray powder diffraction (Figure 5). Here, the as-prepared material exhibits very broad reflections, which nevertheless indicate the presence of cassiterite. Considering the thickness of the crystalline shell, this extreme broadening of reflections is in accordance to the expectation. X-ray diffraction patterns were also recorded for samples annealed at 350 °C for 3 h and at 600 °C for 5 h in air (Figure 5). These patterns indicate a certain increase in crystallinity, but still exhibit broad reflections. Now the material can be valuably identified as cassiterite. On the basis of Scherrer's equation, a crystallite size of 4 nm for the sample annealed at 350 °C was deduced and fits well with the wall thickness gained from HRTEM (Figure 1c, d). Respectively, the crystallite size of the sample annealed at 600 °C is calculated to 12 nm. Altogether, annealing at 350 °C, the highest temperature applied for sensor operation −, does not strongly affect the crystallite size. Even at temperatures up to 600 °C, the crystal growth is limited, though an improved crystallinity is observed and further proves the presence and purity of SnO_2. Note that a high-pressure modification (Figure 1d) is not observed by X-ray diffraction. This can point either to a very low concentration of this modification or to the fact that it is formed under electron bombardment only.

Electron microscopy of the nanoparticle layers treated at 350 °C unfortunately turned out to be difficult. Due to agglomeration and sintering this especially holds for thin, "monoparticulated" layers required for HRTEM to prove the inner cavity of the hollow spheres. XRD, SEM/STEM, and BET, however, clarify the structural properties of the sintered particle layers. According to SEM/STEM images, the sintered nanoparticles exhibit diameters of 15−25 nm and look quite similar to the as-prepared material (Figure 6a, cf. Figure 1a,b). STEM images indicate highly porous layers and suggest the presence of hollow spheres (Figure 6b). As discussed above, the crystallite sizes deduced from XRD (Figure 5) do not show any significant alteration of the sintered sample in comparison to the as-prepared material, too. On the other hand, a significant decrease of the BET surface (119 $m^2 g^{-1}$) is observed. Taking into account that this finding, on the one hand, is not accompanied by crystallite growth and that a potential thermal destruction of hollow spheres, on the other hand, does not necessarily cause a decrease in the specific surface, the situation, in sum, can be ascribed to a thermally induced agglomeration and sintering of particles via their outer surface. This assumption is well in accordance

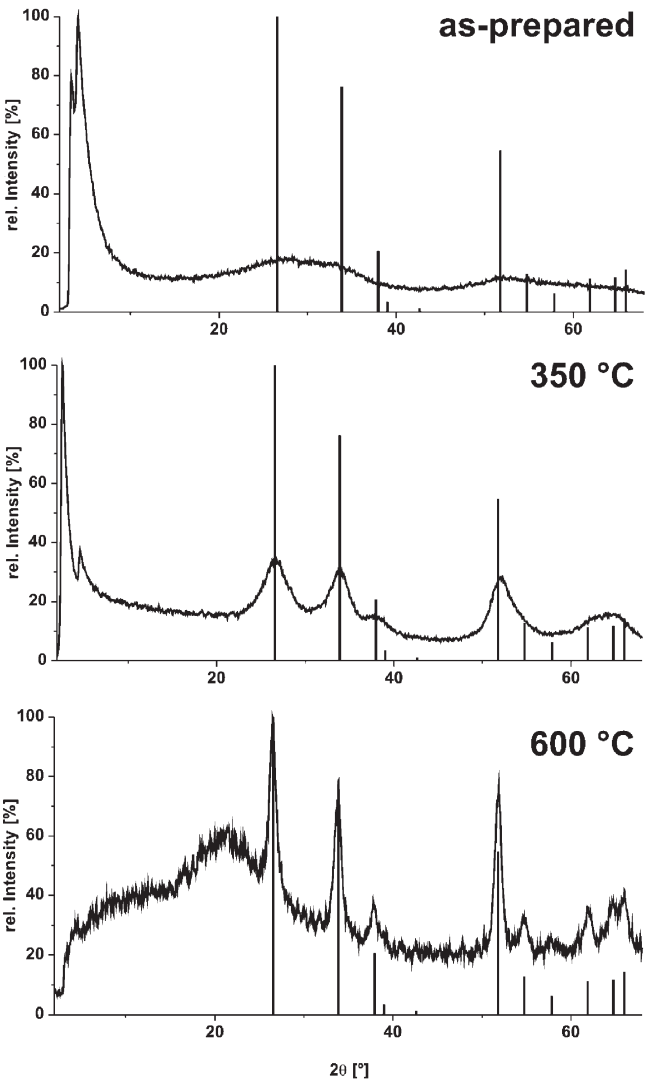

Figure 5. X-ray powder diffraction patterns of as-prepared SnO_2 hollow spheres and the material treated at different temperatures (reference: SnO_2 ICDD-No. 88−287).

with the analytical data as well as with the observed very high brittleness of the sintered layers. The latter, as discussed above, complicates preparing thin films for HRTEM analysis. Finally, the characteristic hysteresis for nitrogen adsorption and desorption is still visible and can also be taken as an indication that the SnO_2 nanoparticles after sintering at 350 °C still contain cavities (Figure 4, Figure 6).

Note that the obtained sensor layers—although a certain decrease of the BET surface was observed—nevertheless exhibit one of the highest specific surfaces obtained for sintered SnO_2 nanoparticles.[6] Such specific surfaces were yet only gained by thermal decomposition of organic−inorganic hybrid precursors such as tin acetates, alkoxides, or acetylacetonates.[24−26] In contrast to these precursors, however, spin-coating or drop-casting of nanoparticle

(23) Chandra, D.; Mukherjee, N.; Mondal, A.; Bhaumik, A. *J. Phys. Chem. C* **2008**, *112*, 8668.
(24) Sedghi, S. M.; Mortazavi, Y.; Khodadadi, A.; Sahraei, O. A.; Naseh, M. V. *Int. J. Chem. Biomol. Eng.* **2009**, *2*, 69.
(25) Toupance, T.; El Hamzaoui, H.; Joussecaume, B.; Riague, H.; Saadeddin, I.; Camper, G.; Brötz, J. *Chem. Mater.* **2006**, *18*, 6364.
(26) Wang, Y.; Ma, C.; Wu, X.; Sun, X.; Li, H. *High-perform. Mater.* **2001**, *224−226*, 225.

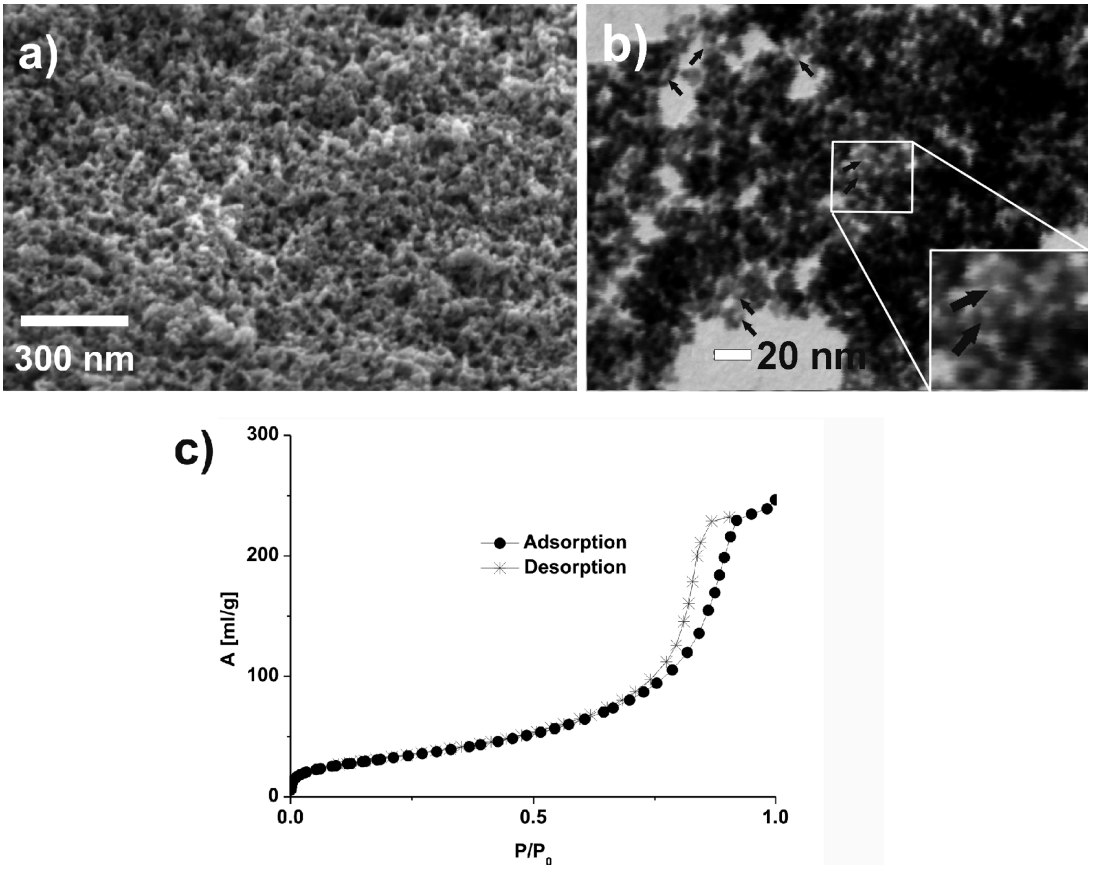

Figure 6. SnO_2 hollow spheres subsequent to annealing at 350 °C in air and sensor operation: (a) SEM and (b) STEM images of the highly porous material (with some nonagglomerated hollow spheres indicated by arrows) and (c) nitrogen sorption analysis.

suspensions is much more straightforward, aiming at low-cost, easy-to-fabricate sensors.

Sensing Performance of SnO_2 Hollow Spheres Material. A sensing layer was established by straightforward procedures: just by dip-coating of as-prepared SnO_2 hollow spheres in ethanol on Al_2O_3 substrates a suitable test device was realized. Figure 7 shows an example of the sensor response to different concentrations of CO (20, 40, 60, 80, 100, 140, 180, 220, 260, and 290 ppm) at a temperature of 350 °C and 300 °C. The testing sequence was started by exposure to humid air for 2 h in order to get a stable baseline resistance followed by several 20 min CO pulses separated by 30 min exposures to the background atmosphere. This measurement procedure was applied twice for both sensor operation temperatures in order to check the reproducibility of the signals.

The sensors based on as-prepared SnO_2 hollow sphere material indeed show a good response toward different CO concentrations at both operation temperatures.[27] After starting the measuring procedure, the equilibrium is reached quite fast and the baseline of the resistance turned out to be stable after 30 min. The response time is very fast (< 1 min), and the full recovery takes place during the allotted 30 min. The effects of temperature increase with 50 °C are a decrease of the baseline resistance and a doubling of the sensor signal (defined as the ratio R_{air}/R_{gas}). The results obtained at both temperatures are shown, in the form of calibration curves, in Figure 8. There, one can observe the typical behavior of semiconducting metal oxide based sensors, namely a

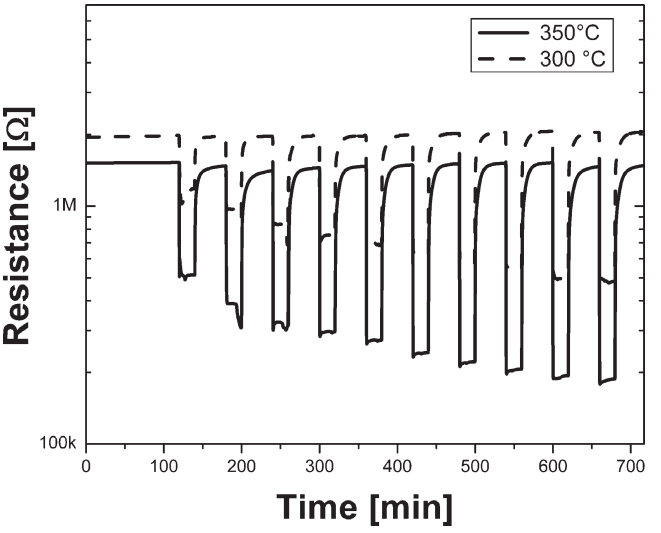

Figure 7. Resistance change of SnO_2 hollow spheres sensor at two different temperatures (300 and 350 °C) during exposure to stepwise increasing CO pulses (20, 40. 60, 80, 100, 140, 180, 220, 260, and 290 ppm) in humid air (50% rel. humidity).

(27) Kappler, J.; Barsan, N.; Weimar, U.; Dièǵez, A.; Alay, J. L.; Romano-Rodriguez, A.; Morante, J. R.; Göpel, W. Correlation between XPS, Raman and TEM Measurements and the Gas Sensitivity of Pt and Pd Doped SnO2 Based Gas Sensors. In *Proceedings of the 9th International Conference on Solid State Analysis*; Chemnitz, Germany, June 23−26, 1997; Springer: New York, 1997;Fresenius' J. Anal. Chem. **1998**, *361*, 110.

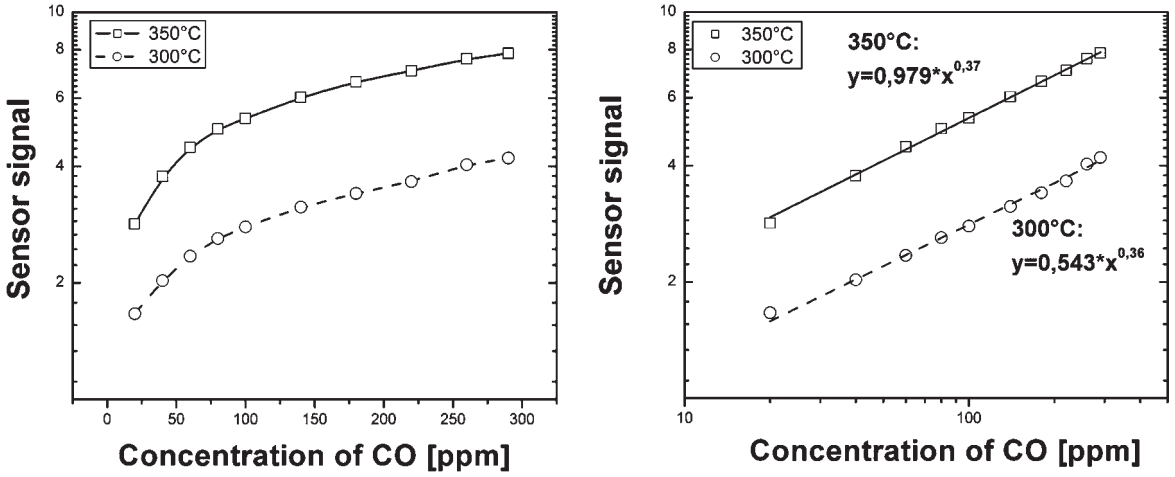

Figure 8. Comparison of sensor signals at different CO concentrations for the two investigated temperatures in single logarithmic (left) and double logarithmic presentation (right); the calibration curves were fitted with a power law dependence.

saturation tendency at higher concentration that indicates a power law dependency of the resistance/sensor signal on the target gas concentration. The actual dependencies are indicated in Figure 8, where the sensor signal dependence on the concentration is shown in double logarithmic plot. One can observe that the exponents are practically identical for both operation temperatures (0.36 and 0.37, respectively), which indicates the same type of sensing reaction (involving the same kind of surface oxygen species).[4] The difference in signal is related to the value of the pre-exponential factor and its significance is not clear at this moment. One has to note that the sensor signal is much lower—almost a factor 10—than the one corresponding to commercial SnO_2-based CO-gas sensors operated.[28,29] This is due to the fact that the very high sensor signals, shown by the commercial devices, are due to the use of surface additives (such as Pd and Pt) and to pulsed temperature operation modes. However, when constant temperature operation modes are employed, the value of the exponent is not too different,[29] which indicates comparable sensitivities (defined as the slope of the calibration curve).[30]

It is possible to compare the results from the obtained power law with the former calculated models for the conduction process. For a porous layer with small grains the modeling gives the followed general dependence for the conductance G and the partial pressure of the target gas:

$$G \approx p_{CO}^{\beta/\alpha+1} \quad (1)$$

where α, singly or doubly ionized forms, and β, atomic or molecular forms, describe the reactive oxygen species at the surface (see Table 1).

In the operation temperature range, the molecular oxygen form on the surface of SnO_2 does not exist anymore.[31,32] Comparing the factors from the performed measurement and the modeling there is somehow an analogy (0.365 compared with 0.33). Hence, it might be permitted to apply the model for complete depletion layers like for small grains. The difference in the exponential factor might originate from a second fact. In the case of such small spheres one should consider also the mean free path of the electrons. If the ratio between the mean free path of the electrons λ and the dimension of the spheres is non negligible, the surface phenomena influence not only the concentration of electrons but also the mobility. The overall conductance is, accordingly, affected by changes in the concentration of the electrons and in their mobility, caused by surface scattering. To consider the additional effect one has to correct the common dependence between the conductance and the concentration of the target gas with a common factor. This can be done as followed:[4]

$$G \approx (p_{CO}^{\beta/\alpha+1} + \text{const} p_{CO}^{2\beta/\alpha+1}) \quad (2)$$

The second part of the formula describes the influence of change in mobility of the electrons. The constant depends on the geometrical and electrical properties of the material.

Table 1. Summary of the Different Power Laws Obtained by Modeling for Small Grains

reactive oxygen species	α	β	power law
O_2^-	1	2	$G \approx p_{CO}$
O^-	1	1	$G \approx p_{CO}^{0.5}$
O^{2-}	2	1	$G \approx p_{CO}^{0.33}$

Conclusions

The studied SnO_2 hollow sphere material deposited on a common sensor substrate show a good sensor response to CO in a concentration range that is relevant to applications.[33] The sensing procedure and the translation into an electrical signal for SnO_2-based sensors are very complex phenomena. The factors, namely surface reactions, charge transfer processes, and morphology, determine

(28) http://www.figarosensor.com.
(29) http://www.appliedsensor.com.
(30) Barsan, N.; Stetter, J. R.; Findlay, M.; Göpel, W. *Anal. Chem.* **1999**, *71*, 2512.
(31) Lenaerts, S.; Roggen, J.; Maes, G. *Spectrochim. Acta, A* **1995**, *51*, 883.
(32) Yamazoe, N.; Fuchigami, J.; Kishikawa, M.; Seiyama, T. *Surf. Sci.* **1979**, *86*, 335.
(33) http://www.enius.de/schadstoffe/kohlenmonoxid.html

the relation between the conductance and the partial pressure of the target gas. In the case of hollow sphere material, one obtains from the measurement a dependence like $G \approx p_{CO}^{0.365}$. This obtained value is comparable with the one from the conduction model for a porous layer with small grains. Furthermore, the influence of surface scattering has to be taken in consideration for the modeling depending on the ratio between the mean free path of the electrons and the dimensions of the spheres. In the case of the hollow spheres, the latter ratio might be non negligible and the influence of surface phenomena in overall conductance will originate from mobility and concentration of electrons n_S. Finally the conductance dependence to the partial pressure of CO is not simply caused by the electron concentration. There is an additional factor describing the mobility influence, which also contributes to the exponential factor in the received power law. The common conduction model should also be valid for the hollow spheres material.

As a result of our fundamental study, we do see a potential of the newly prepared SnO_2 hollow spheres with regard to a technical sensor. To be comparable with a real sensor device, however, the use of surface additives (such as Pd and Pt) is necessary as a next step. In addition to the excessive surface, here, the special morphology of the hollow spheres might be advantageous upon a higher degree of freedom. In fact, surface additives can be attached to the inner or the outer or both types of surfaces.

Acknowledgment. The authors are grateful to Dr. R. Popescu and Prof. Dr. D. Gerthsen for performing TEM analysis. We further acknowledge the DFG Center for Functional Nanostructures (CFN) at the University of Karlsruhe (TH) for financial support.